Molecular Dynamics of Photosystem II Embedded in the Thylakoid Membrane

van Eerden, Floris Jan; van den Berg, Tom; Frederix, Pim; de Jong, Djurre H; Periole, Xavier; Marrink, Siewert

Published in:
Journal of Physical Chemistry B.

DOI:
10.1021/acs.jpcb.6b06865

Publication date:
2017

THE JOURNAL OF PHYSICAL CHEMISTRY B

Article

pubs.acs.org/JPCB

Molecular Dynamics of Photosystem II Embedded in the Thylakoid Membrane

Floris J. van Eerden,[†] Tom van den Berg,[‡] Pim W. J. M. Frederix,[†] Djurre H. de Jong,[†] Xavier Periole,[†] and Siewert J. Marrink*[,†]

[†]Groningen Biomolecular Sciences and Biotechnology Institute & Zernike Institute for Advanced Materials, University of Groningen, Nijenborgh 7, 9747 AG, Groningen, The Netherlands

[‡]Department of Physics and Astronomy, Faculteit der Exacte Wetenschappen, Vrije Universiteit, De Boelelaan 1081, 1081 HV Amsterdam, The Netherlands

Supporting Information

ABSTRACT: Photosystem II (PSII) is one of the key protein complexes in photosynthesis. We introduce a coarse grained model of PSII and present the analysis of 60 μs molecular dynamics simulations of PSII in both monomeric and dimeric form, embedded in a thylakoid membrane model that reflects its native lipid composition. We describe in detail the setup of the protein complex and the many natural cofactors and characterize their mobility. Overall we find that the protein subunits and cofactors are more flexible toward the periphery of the complex as well as near the PLQ exchange cavity and at the dimer interface. Of all cofactors, β-carotenes show the highest mobility. Some of the β-carotenes diffuse in and out of the protein complex via the thylakoid membrane. In contrast with the PSII dimer, the monomeric form adopts a tilted conformation in the membrane, with strong interactions between the soluble PsbO subunit and the glycolipid headgroups. Interestingly, the tilted conformation causes buckling of the membrane. Together, our results provide an unprecedented view of PSII dynamics on a microsecond time scale. Our data may be used as basis for the interpretation of experimental data as well as for theoretical models describing exciton energy transfer.

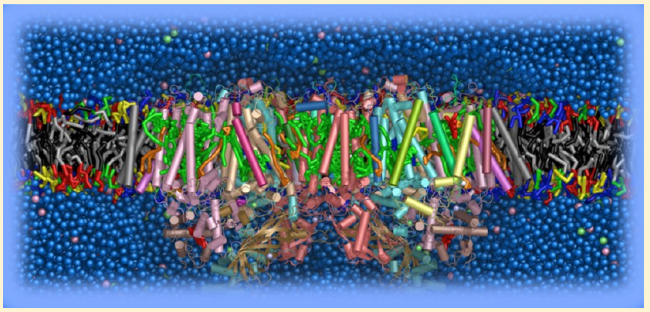

INTRODUCTION

Photosynthesis is the extremely important process in which the energy of photons is converted into chemical energy. Photosystem II (PSII), a protein complex located in the thylakoid membrane of cyanobacteria and plants, is a main component in this process. PSII uses chlorophylls and carotenoids as antennas to capture photons. The energy of the photons is used to oxidize water and to subsequently reduce plastoquinone (PLQ), which renders oxygen as a waste product. Concurrently a proton gradient is generated, which is used for the generation of adenosine triphosphate (ATP).[1,2]

PSII is a homodimer in vivo, but individual monomers are fully functional.[3] The PSII complex is large; each monomer consists of 27 subunits in plants and 20 in cyanobacteria, respectively.[4] A large number of cofactors supplement PSII with its light-harvesting and water-splitting capabilities. Each monomer contains around 77 cofactors, including ions and a number of glycolipids.[5−7] More details of the structure and functioning of PSII can be found in a number of recent reviews.[4,8−13]

Studying the dynamics of proteins and lipids is challenging, as relevant time and length scales are not easily accessed experimentally. Molecular dynamics (MD) simulations can contribute to the elucidation of cellular processes by providing a detailed and dynamic view on protein−lipid interactions.[14−16] In the case of photosynthesis, the Schulten laboratory has pioneered the use of MD, often in combination with other structural techniques, to elucidate the organization of various light-harvesting complexes. Sener et al., for instance, created an all-atom model of a bacterial chromatophore by merging AFM, cryo-EM, and crystallography data.[17] The model was subsequently used to explore energy transfer across the surface of this organelle. In another example, Chandler et al. studied the excitation transfer rates in a big patch of the photosynthetic membrane of a purple bacterium by combining MD and quantum dynamics.[18]

Concerning PSII, atomistic simulations have been performed by a number of groups, with a primary focus on the movement of water through the protein complex. For instance, Vassiliev et al. identified a branched network of water channels in PSII and compared the water flow in the presence and the absence of the oxygen evolving complex (OEX).[19] In a later study the energy

Special Issue: Klaus Schulten Memorial Issue

Received: July 11, 2016
Revised: September 13, 2016

DOI: 10.1021/acs.jpcb.6b06865
J. Phys. Chem. B XXXX, XXX, XXX−XXX

profiles for water penetration into water channels were calculated and sites that might function as selectivity filters were identified.[20] Gabdulkhakov et al. also studied the water channels in PSII and assessed the mobility of water molecules in the different channels.[21] Ogata et al. performed an all-atom simulation of PSII embedded in a model of the thylakoid membrane. They analyzed the diffusion of lipids and studied the transfer of water, protons, and oxygen along different pathways.[22] In another study, Zhang et al. used QM/MM to determine the excitation energy of chlorophylls at the PSII reaction center[23] and identified chlorophyll *a* (CHL) 606 as the most probable site for energy excitation.

Despite the significance of these studies, the time scales probed in the simulations are limited to the nanosecond range, while many processes in PSII take place on much longer time scales, for example, PLQ exchange and the PSII repair cycle. Current computational power makes it difficult to study the dynamics of big protein complexes like PSII with atomistic detail on a microsecond time scale. Coarse grain (CG) force fields, in which some of the atomistic details are averaged out, allow one to go beyond the limitations of the atomistic models.[24,25] In particular the CG Martini force field[26] has been widely applied in this area, for example, to predict protein−lipid binding sites,[27,28] to study membrane mediated protein−protein interactions,[29−31] and to explore the role of compositional complexity and crowding.[32−34]

Here we present CG simulations of PSII from cyanobacterium *Thermosynechococcus vulcanus* based on the Martini force field. The complex is embedded in a realistic thylakoid membrane[35] composed of a mixture of phosphatidylglycerol (PG), and the glycolipids digalactosyldiacylglycerol (DGDG), monogalactosyldiacylglycerol (MGDG) and sulfoquinovosyldiacylglycerol (SQDG) glycolipids. We describe in detail the setup of this complex system and present results on the internal mobility of the protein subunits and various cofactors for both the PSII monomer and dimer. Our simulations provide a dynamic picture of the PSII complex that can serve as a reference for refined calculations of exciton transport in these systems and are an important step toward detailed simulations of large-scale supercomplex formation of the photosystem and its antenna complexes.

METHODS

Simulation Parameters. The Martini force field (version 2.2) was used to model the protein interactions.[36] The ElNeDyn approach was used to stabilize the protein[37] using the standard values for cutoff = 0.9 nm and force constant F_c = 500 kJ mol^{-1} nm^{-2}. ElNeDyn defines a network of elastic bonds between the backbone beads (BBs) of residues of the same subunit that are within the cutoff distance. It should be stressed that the different PSII subunits are not bonded to each other in any way, so they are free to move independently. The lipid parameters were based on the parameters for glycolipids from López et al.[38] with slight modifications as described by van Eerden et al.[39] The parameters for the cofactors were taken from de Jong et al.,[40] with a few modifications to improve numerical stability (see Supporting Information, Figure S1). The standard Martini water model was used,[41] in which four real water molecules are represented by a CG bead.

The GROMACS 4.5.5 MD package[42] was used to perform the simulations, with the standard parameter settings for the Martini force field.[41] The system was simulated using the isothermal−isobaric (NpT) ensemble. The v-rescale thermostat was used to control the temperature with a coupling constant τ_t = 2.0 ps.[43] The pressure was semi-isotropically coupled to an external bath of p = 1 bar with a coupling constant of τ_p = 1.0 ps and compressibility of $\chi = 3.0 \times 10^{-4}$ bar^{-1} using the Berendsen barostat.[44] The electrostatic interactions were calculated using a shifted potential with a cut off of 1.2 nm and a dielectric constant of 15. For the calculation of the van der Waals interactions a shifted potential was also used, with a cut off of 1.2 nm and a switch at 0.9 nm.

Setup of the PSII Complex. The crystal structure of PSII of the thermophilic cyanobacterium *Thermosynechococcus vulcanus* served as the starting structure of the simulation, PDB ID: 3ARC.[6] (Note, a refined version of the Umena structure had been released, PDB ID: 3WU2, which supersedes entry 3ARC in both the PDB and OPM databases.) The structure contains 19 out of a total of 20 subunits. The two monomers of the crystal structure are virtually identical, except for some slight variations in the loop regions. We therefore decided to prepare only the first monomer of the pdb file and, after its setup, copy it to the position of the second monomer. Missing residues were reconstructed using Swiss-PdbViewer,[45] ModLoop,[46] and VMD.[47] VMD's Molefacture extension was used to model missing heteroatoms back in the structure. After the reconstruction of all the residues, a dimer was obtained by fitting the now reconstructed first monomer on the second monomer using the Multiseq extension in VMD.

Membrane proteins usually have a preferred positioning in the membrane. To prepare PSII for insertion in a bilayer, it was fitted on the 3ARC entry of the OPM database[48] with the use of PyMol.[49] The OPM database contains a calculated orientation of membrane proteins in the bilayer. The Martinize script[36] was then used to convert the protein part of PSII (i.e., the amino acids) to a CG Martini structure, with DSSP[50] being used on the fly to determine the secondary structure of the protein. In the Martini model the polarity of the BBs and the dihedral between BBs depends on the secondary structure, which therefore remains fixed during the simulation.[51] All histidines were modeled in their neutral form.

Only after the reconstruction of the second monomer and the CGing of the dimer was it noted the missing residues of the cyt b 559β, residues 2−11, were not correctly modeled by ModLoop. The positions of these residues were therefore manually adjusted in VMD, separately for each monomer. This resulted in small differences between the two monomers in the coordinate file of the starting structure; the topology is, however, identical for the two monomers.

Inclusion of Cofactors. The PSII crystal structure contains a large number of cofactors: CHL, pheophytin (PHO), heme (HEM), β-carotene (BCR), PLQ, and the OEX, displayed in Figure 1. An overview of the number of each of these cofactors, as well as cocrystallized ions, is given in Table 1. All cofactors were explicitly included in our simulation, as shown in Figure 2. In this study the CHL cofactors are numbered as in Umena et al., which is their residue number in the pdb file minus 600. According to this scheme we also numbered the HEM and PHO cofactors. The other cofactors are identified according to the residue number that they have in the structure of Umena et al.[6]

In vivo the HEM and CHL molecules in PSII are coordinated to the protein by a lone-pair interaction. This lone-pair interaction is between the central metal ion and the coordinating amino acid or water molecule. Of the 35 CHLs that are present in a monomer, 27 are coordinated by

DOI: 10.1021/acs.jpcb.6b06865
J. Phys. Chem. B XXXX, XXX, XXX−XXX

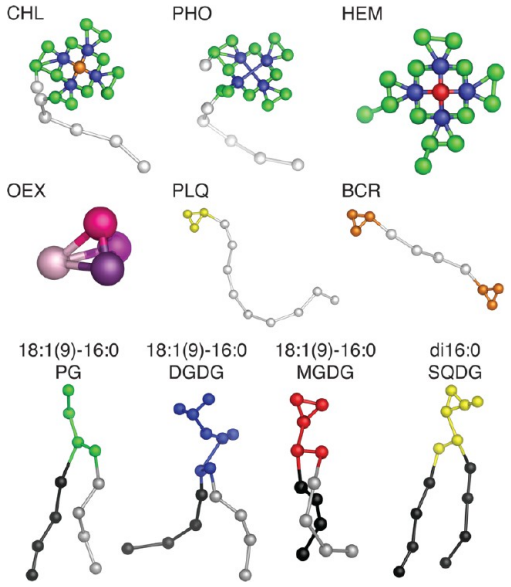

Figure 1. CG models of cofactors and lipids associated with PSII. The tails of CHL, PHO, PLQ, and BCR are colored white. Palmitoyl tails of lipids are colored black and oleoyl tails gray. The headgroups and glycerol linkers of the different lipid types are colored uniquely to distinguish them in subsequent figures. The OEX beads are colored differently for clarity only. Note that the lipids and cofactors are not drawn to scale.

Table 1. List of the Cofactors That Are Included in the Simulation[a]

cofactor name	abbreviation	number per monomer
chlorophyll *a*	CHL	35
pheophytin	PHO	2
heme	HEM	2
β-carotene	BCR	12
plastoquinone	PLQ	2
oxygen evolving complex	OEX	1
nonheme iron	Fe^{2+}	1
water (for CHL coordination)	W	5
magnesium ion	Mg^{2+}	1
bicarbonate ion	BCT	1
calcium ion	Ca^{2+}	3
chloride ion	Cl^{-}	3

[a]Numbers are per monomer. The lipids are not included in this list.

histidines, 7 by water molecules, and 1 by an asparagine residue. The two HEMs are coordinated by two histidine residues each. The Martini force field does not take into account lone-pair interactions. To mimic the coordination of the cofactors, every CHL and HEM molecule was bound to its coordinating residues with harmonic bonds; see the Supporting Information (Tables S1 and S2 and Figure S2).

PHOs do not have a central ion by which they can be ligated to the protein. The PHOs, however, showed relatively large and unrealistic movements during our preliminary simulations. To reduce this behavior the PHOs were also linked to the complex with harmonic bonds; see the Supporting Information (Tables S1 and S2) for details. For BCRs and PLQs, no bonded potentials were used to tie them to the protein complex.

The OEX is an essential part of the PSII system in which the water splitting occurs. Our CG model of OEX is, of course, not capable of capturing any chemical reactions, but it does give a

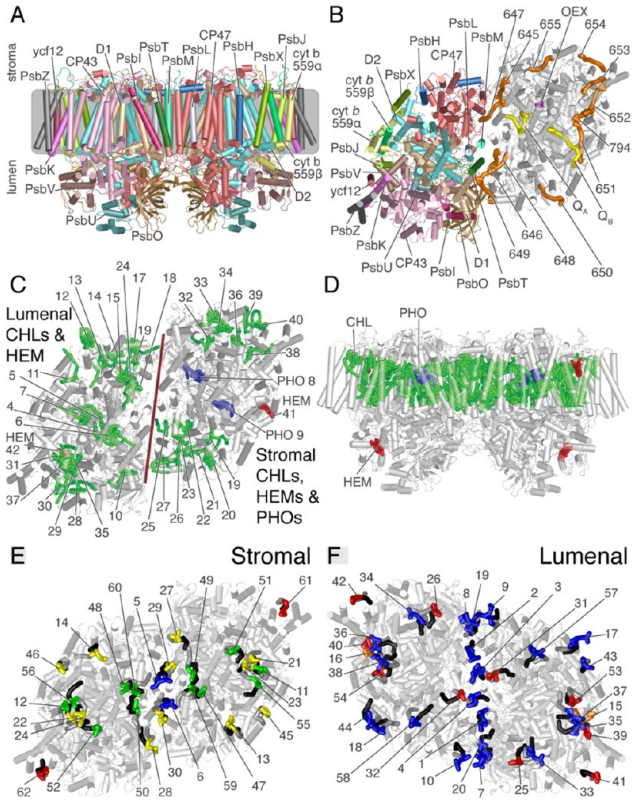

Figure 2. Position of PSII subunits and cofactors. (A) View on PSII dimer from the plane of the membrane, with labeling of the 19 subunits colored according to chain. The gray box roughly indicates the position of the thylakoid membrane. The top of the picture corresponds to the stromal side of the thylakoid membrane and the bottom to the lumenal side. (B) Stromal view on the PSII dimer with all cofactors except chlorophyll *a* (CHL), pheophytin (PHO), and heme (HEM). The left monomer is colored and labeled as in panel A. In the right monomer the protein is colored transparent white and the cofactors are shown. The cofactors are colored as follows: plastoquinone (PLQ) yellow (in Qa and Qb sites), *β*-carotene (BCR) orange, and oxygen evolving complex (OEX) purple. The BCRs are labeled with the residue numbers they have in the crystal structure of Umena et al.[6] (C) Stromal view of the PSII dimer showing the lumenal and stromal positioned CHLs, PHOs, and HEMs. The protein is shown in transparent white, CHL in green, PHO in blue, and HEM in red. The left monomer shows the lumenal positioned CHLs and HEM and the right monomer shows the stromal CHLs, PHOs, and HEM, which are all labeled according to their identifier. (D) Side view of the PSII dimer with all CHL and PHO, coloring as in panel C. Stromal (E) and lumenal (F) view of all lipids included in the PSII dimer model. Lipids 1–20 are cocrystallized detergents and unassigned lipids that were replaced by designated lipids (or BCR in case of lipids 15,16), lipids 21 and 22 were added for structural stability, and lipids 23–62 are cocrystallized lipids found in the crystal structure; for details see Table S3. Coloring as in Figure 1.

representation of the space the OEX occupies as well as of its overall charge of +6e. We modeled the OEX by a cluster of four Q0 beads with a charge of +1.5e each. The beads are bound to each other with harmonic bonds with F_c = 10 000 kJ mol^{-1} nm^{-2}. In vivo the OEX is coordinated by a combination of water molecules and amino acids, whereby the latter neutralize the charge of the OEX. In the CG system the OEX is also neutralized by amino acids. Stable coordination is achieved through a number of harmonic bonds; see the Supporting Information (Tables S1 and S2).

DOI: 10.1021/acs.jpcb.6b06865
J. Phys. Chem. B XXXX, XXX, XXX−XXX

Furthermore, we included all cocrystallized ions in our systems as well as the special bicarbonate ion, which is thought to be important for electron transport[52] (cf. Table 1). To model the cations (Mg^{2+}, Fe^{2+}, Ca^{2+}), for which no standard Martini parameters exist, a Q0 particle type was used with a $+2e$ charge. The bicarbonate ion was modeled as a Qda particle with $-e$ charge. Note that Martini treats ions in a rather qualitative way. Except for their role in coordination, in this study ions do not play an important role, and no attempt was made to optimize the parameters. The cocrystallized ions were ligated to the PSII system with harmonic bonds; see the Supporting Information (Tables S1 and S2). The PSII structure also contains many cocrystallized water molecules. In the Martini model, a water bead represents four real water molecules, which makes it impossible to include individual water molecules into our model. Therefore, all water molecules were deleted from the structure. Most crystallized waters are found in the soluble domains of the PSII complex and in the solvent-accessible PLQ exchange cavity, and these get rehydrated in the simulation during the equilibration phase. Some water molecules are present in the interior of the complex, for example, playing a role in ligation of CHL, and their stabilizing role is mimicked by harmonic bonds (see above).

All cofactors were coarse grained independently from the protein using the Backward script.[53] The position of the cofactors inside PSII is illustrated in Figure 2B–D.

Inclusion of Cocrystallized Lipids. Four different types of lipids are present in the crystal structure: the negatively charged lipids PG and SQDG and the neutral MGDG and DGDG; see Figure 1. All 40 cocrystallized lipids were included in the simulation; an overview is given in Supporting Table S3. The position of the lipids inside the PSII dimer is shown in Figure 2E,F. The lipid tails are not resolved in the crystal structure and were modeled with an 18:1(9) (oleoyl) tail at the *sn*-1 position and a 16:0 (palmitoyl) tail at *sn*-2, in accordance with the fatty acid composition of the thylakoid membrane as determined by Sakurai et al.[35] Details of the specific lipids included in our model in the case of detergent molecules or poorly resolved lipid densities are given in the Supporting Information.

Embedding in the Thylakoid Membrane. The complete PSII dimer, including all cofactors, cocrystallized ions, and internal lipids, was subsequently embedded in a CG model of the thylakoid membrane of *T. vulcanus* and solvated using the *Insane* script.[54] The composition of the membrane was taken from van Eerden et al.,[39] which is an adaptation to CG resolution of the lipid composition experimentally determined by Sakurai et al.[35] The thylakoid membrane contains 2686 lipids in total, comprising a mixture of MGDG, DGDG, SQDG, and PG lipids, as specified in Table 2. A smaller bilayer, containing 1425 lipids, was used to solvate the PSII monomer. Compared with the composition of Sakurai et al., our membrane contains a slightly increased amount of PG lipids to increase the probability of observing interactions between PSII and PG. Experimental evidence indicates that these might be important.[35]

The *Insane* script was invoked to give all lipid beads a random kick of 0.05 nm, and periodic images were separated by 10.5 nm in the *xy* dimension and 18.0 nm in the *z* dimension. This resulted in a rectangular box with a square base in the membrane plane with dimensions of 30.8 × 30.8 × 14.4 nm in the *x*, *y*, and *z* dimensions. A similar procedure for the monomer system resulted in a box of 22.5 × 22.5 × 14.0 nm. The dimer/monomer systems were, respectively, solvated with 73 144/40 648 CG water beads (representing four times as many water molecules). In addition, 455/253 Na^+ and 455/253 Cl^- ions were added, corresponding to ∼100 mM Na^+Cl^- plus 1032/541 Na^+ counterions to neutralize the overall charge.

Table 2. Composition of the Thylakoid Membrane[a]

		dimer		monomer	
		number of lipids			
lipid name	mol %	stromal leaflet	lumenal leaflet	stromal leaflet	lumenal leaflet
18:1(9)-16:0 PG	10	134	134	71	71
18:1(9)-16:0 DGDG	25	336	336	179	178
18:1(9)-16:0 MGDG	40	538	538	287	284
18:1(9)-16:0 SQDG	15	201	201	107	106
Di16:0 SQDG	10	134	134	71	71

[a]Note that in the current study the amounts of unsaturated and fully saturated SQDG were slightly adjusted to better match the experimental data from Sakurai et al.,[35] with respect to the values used previously.[39] This means that 15% of all lipids are 18:1(9)-16:0 SQDG and 10% of the lipids di16:0 SQDG versus, respectively, 10 and 15% in the study of Van Eerden et al. Note that in the monomer the lumenal membrane leaflet contains a few lipids less than the stromal leaflet. The Insane-script[53] assigns the number of lipids per leaflet based on the available space. The fact that the lipid amount of the lumenal leaflet is slightly smaller reflects that the lumenal side of the monomer is slightly larger than the stromal side.

Equilibration and Production Runs. After solvation, both the dimer and monomer systems were energy-minimized using three different minimization steps. First a steepest descent minimization was performed, followed by a conjugate gradient and then a second-steepest descent minimization. Both systems were subsequently equilibrated in eight consecutive runs totaling 298 ns, in which the time step was slowly increased from 1 to 10 fs and the temperature was increased from 200 to 328 K. During the minimization and the equilibration runs, position restraints were applied on the protein backbone and the cofactors with a force constant of 1000 kJ mol^{-1} nm^{-2}.

For the production runs, no restraints were applied. The PSII dimer and the monomer were both simulated for 60 μs at T = 328 K. The first 1 μs was discarded as further equilibration time, rendering a total analysis time of 59 μs. The trajectories were saved every 1 ns. Details of the analysis (calculation of root-mean-square fluctuations (RMSFs) of the protein subunits and cofactor and protein diffusion constants) are given in the Supporting Information.

In addition, five replicate simulations of the dimer system with different seeds for the initial randomized velocities were performed. The replica simulations had a length of between 80 and 100 μs each, extending the total simulation time by 475 μs. These simulations had the same starting structure as described before but contained PLQ in the membrane and PLQol at the Q_B site to study the diffusion of these cofactors, to be addressed in a separate paper. Here we use these replicate simulations to increase the statistics of some rare events.

RESULTS AND DISCUSSION

We simulated the PSII monomer and dimer complexes of *T. vulcanus* for 60 μs. The complexes contained all cofactors and were embedded in a realistic representation of the thylakoid membrane, shown in Figure 3. *T. vulcanus* is a thermophile;[55] therefore, the simulations were performed at 328 K, maintaining the thylakoid membrane in the fluid phase.[39] In

DOI: 10.1021/acs.jpcb.6b06865
J. Phys. Chem. B XXXX, XXX, XXX−XXX

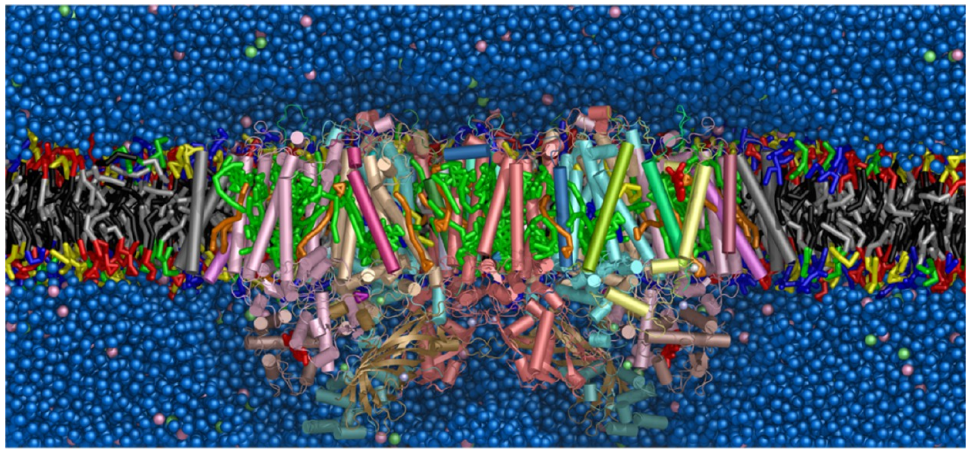

Figure 3. Snapshot of the PSII dimer and all cofactors embedded in a thylakoid membrane. PSII is colored as in Figure 2A and the cofactors as in Figure 2B–D: CHL in green, PHO in blue, HEM in red, PLQ in yellow, BCR in orange, and OEX in purple. The thylakoid lipids are colored as follows: PG head groups in green, DGDG head groups blue, MGDG head groups red, SQDG head groups yellow, oleoyl tails gray, and palmitoyl tails white (cf. Figure 1). Sodium and chloride ions are colored pink and lime, respectively. Water is colored blue. Some water and lipid molecules are omitted for clarity.

the following section we analyze the protein and cofactor mobility of the PSII dimer, after which we will discuss the differences between the monomer and dimer.

PSII Core Shows Limited Flexibility. The internal flexibility of the complex was determined by calculating the root-mean-square deviation (RMSD), with the starting structure before energy minimization used as reference, and the RMSF of the protein backbone (BB), where the reference structure is the time-averaged BB structure. The two monomers reorient slightly in the beginning of the simulation (<1 μs), but the complex remains a stable dimer. The RMSD of the complex stabilizes around ∼0.5 nm after only ∼20 μs and shows that one of the monomers is slightly less mobile; see the Supporting Information (Figure S3). In Figure 4 the residues of the PSII dimer are colored according to their RMSF values. The average RMSF values of the individual subunits are listed in Table S4. The average RMSF is 0.14 nm with a maximum value of 0.77 nm for the PsbX subunit, the latter value resulting from PsbX movement around the protein complex; see below. Note the relative symmetric distribution of RMSF values over the two monomers, indicative of proper sampling of the relative subunits motions over the time period of 60 μs. Full convergence would, however, require more sampling.

Overall the RMSF depicts a relatively rigid protein, especially the transmembrane region of the four big subunits in the core of the complex, D1, CP47, CP43, and D2, while the smaller subunits have a higher RMSF. A high stability of the four big protein subunits, D1, CP47, CP43, and D2, might be important to maintain a proper coupling between all the chlorophylls, thereby ensuring that all excitations arrive at the PSII reaction center.

The flexibility of the PSII dimer in our simulation shows a similar pattern as in the all-atom simulation performed by Ogata et al.[22] They observe very stable helices in the protein core and more mobile regions in the protein periphery such as the stromal exposed residues, the lumenal subunit PsbO, and some of the more peripheral-located transmembrane helices. The fluctuations in our simulations are, however, up to four times as large, which we attribute to the difference in time scales: the all-atom simulation probes dynamics on a time scale of 10 ns, whereas in our simulations the time scale is more than 3 orders of magnitude longer. It is likely that a time scale of 10 ns is too short for the fluctuations to fully develop.

We were not able to find any experimental studies on the dynamics of the individual PSII subunits in vivo or in vitro. However, the crystallographic B factors are often used to discuss mobility of protein main and side chains. This approach, however, should be used with caution, as B factors, in principle, show the uncertainty in the positions of atoms, and that can occur due to numerous reasons: true dynamic behavior, radiation damage, low-quality crystal leading to low-quality data, suboptimal refinement procedure, and so on.[56] Keeping these precautions in mind, we analyzed B factor distribution of the PSII crystal structure at 1.95 Å resolution resolved by of Umena et al.[6] At this resolution, B factors, in general, reflect reliably the dynamics of the system, and they revealed a similar image of the protein mobility compared to our simulations. The peripheral helices and solvent exposed residues have a higher mobility than the residues in the core. A difference with the simulations is that in the crystal structure the helices at the dimer interface do not show an increased mobility. Apparently, embedding the PSII dimer in a bulk membrane environment as apposed to a crystal allows the dimer some freedom to relax the dimer packing. Also of interest is the fact that in both the simulations and the crystal structure the helices of PsbZ become more mobile toward the lumen.

Regions of Increased Mobility: PLQ Exchange Cavity, Periphery, and Dimer Interface. The helix termini are the most mobile parts of the subunits, this is particularly true at the stromal side of the complex. Looking in more detail, we observe somewhat higher transmembrane mobility at three different regions in the complex. The first region with increased mobility is formed by the helices at the peripheral side of the PLQ exchange cavity, cyt b 559α, cyt b 559β, PsbJ, PsbK, and ycf12. The high mobility of PsbJ is remarkable; this subunit delineates together with cyt b 559α one of the PLQ pathways.[57] It has been shown that PsbJ is involved in the downstream electron flow from Q_a to the PLQ pool.[58,59] Its high mobility might be related to the regulation of the PLQ and PLQol exchange to and from the PLQ pool.

The helices located at the periphery of the complex form the second region with increased mobility, notably, PsbI, PsbH,

DOI: 10.1021/acs.jpcb.6b06865
J. Phys. Chem. B XXXX, XXX, XXX−XXX

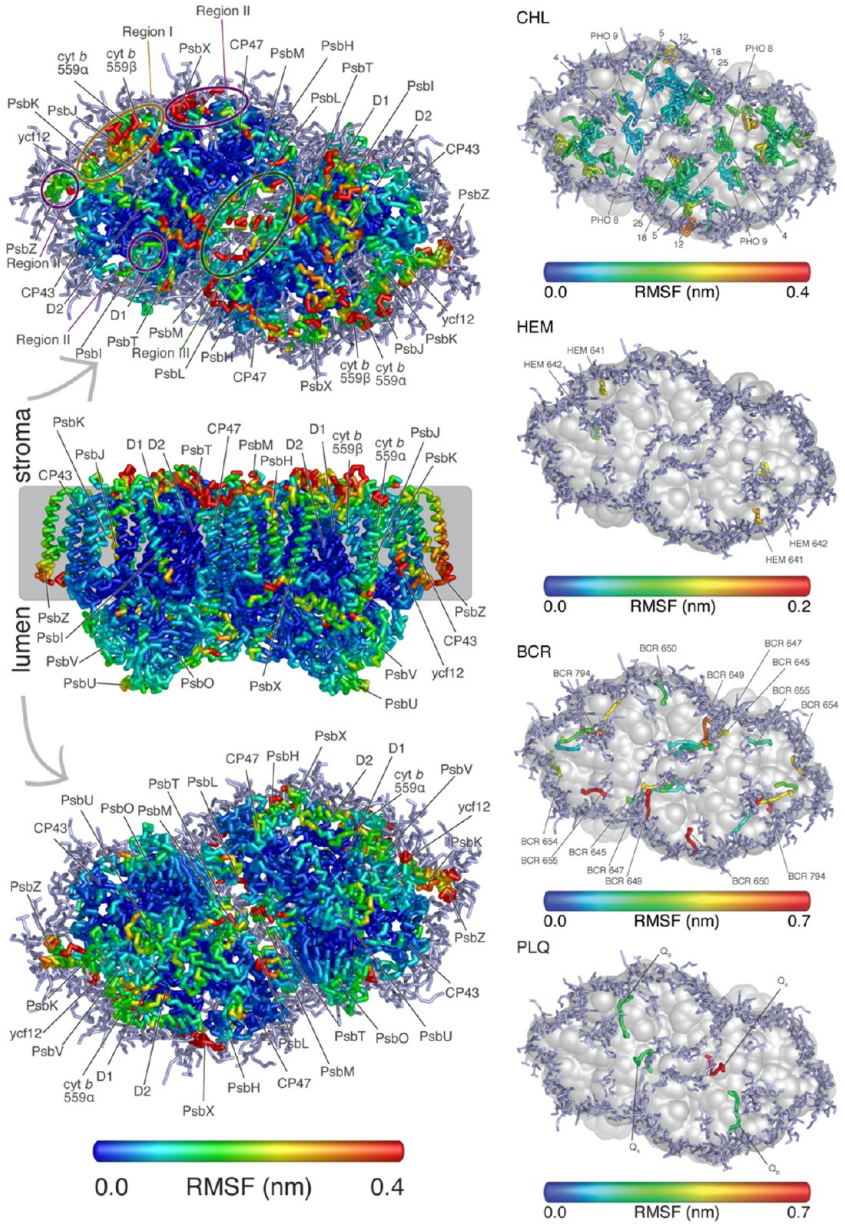

Figure 4. RMSF fluctuations of the PSII backbone (left) and the cofactors (right). The left side shows the fluctuations of the PSII backbone. The various subunits are marked, and the three regions of higher mobility that are discussed in the text are indicated by the circles (region I in yellow, region II in purple, and region III in green). Note that region II is composed of three different areas. The PSII backbone is colored according to RMSF values, which are capped at 0.4 nm. Lipids close to the protein are shown in light blue in the stromal and lumenal views. Right side shows the fluctuations of the different cofactors. First panel: chlorophyll *a* (CHL) and pheophytin (PHO). Second panel: heme (HEM). Third panel: *β*-carotene (BCR). Fourth panel: plastoquinone (PLQ). Each cofactor is colored according to the average RMSF of the complete cofactor. All panels show a stromal view of PSII, with the protein rendered as a transparent surface. For clarity the RMSF values are capped at 0.4, 0.2, and 0.7 nm for CHL/PHO, HEM, and BCR, respectively. The PLQ RMSF values are not capped. Lipids close to the protein are shown in light blue. The cofactors are labeled with their identifier; in the first panel only the CHL and PHO cofactors that are mentioned in the text and are labeled.

PsbX, and PsbZ. In one of the monomers PsbX dissociates from the complex and moves over the protein surface in the direction of PsbH, ending at the interface between PsbH and CP47, in front of CHL 12. This movement explains the high RMSF value of the subunit. Looking at the five replicate simulations, 3 out of 10 PsbX helices show a very similar movement. PsbX is located next to the second PLQ channel,[5] and experiments suggest that this subunit is also involved in the PLQ turnover at the Q_B site.[58,60] Its location and mobility could render PsbX a function as a gatekeeper of the second PLQ exchange pathway. By obstructing the channel, it could influence the flux of PLQ turnover.

The third region with increased mobility is formed by the helices at the dimer interface, of which PsbL, PsbM, and PsbT are the most mobile subunits. The dimer interface is occupied by lipids, which give the neighboring helices some extra conformational freedom and might assist in the formation and dissociation of dimers.[61] PsbM has been suggested to play a key role in the dimerization of PSII[62] by forming a leucine zipper with the PsbM helix from the other monomer.[5] There are experimental results that support the role of PsbM in

DOI: 10.1021/acs.jpcb.6b06865
J. Phys. Chem. B XXXX, XXX, XXX−XXX

dimerization,[63] but other studies suggest that PsbM is not essential for dimerization.[64−66] A possible role for PsbM in dimerization is that it could serve as a recognition element for the reassembly after D1 replacement.[61] During the simulation the PsbM helices stay together at their termini, but the central parts of the helices start to move apart from each other after ∼20 μs. At the beginning of the simulations the PsbM Leu16 side chains are 0.67 nm apart, but the average distance after 50 μs is 1.03 nm. The acyl chains of the lipids wriggle in the space between the two PsbM subunits. In five from a total of six simulations the PsbM helices separate, showing that the contacts between the opposing PsbM helices are not very strong. Our results therefore suggest that PsbM is not needed for the stabilization of the dimer once the dimer has formed. PsbM can, however, still be involved in the actual process of dimerization. Weak interactions between the PsbM subunits are in line with the fact that the PSII has to monomerize during the D1 repair cycle,[67] which would be impaired by too strong connections between the monomers.

Isolated PSII Complex Diffuses Relatively Fast. To measure the mobility of the entire complex, we calculated the lateral translational diffusion constant. The translational diffusion constant of the dimer, obtained from the slope of the mean-squared displacement of the PSII dimer over time (Figure S4), is 2.7 ± 0.2 $\mu m^2\ s^{-1}$. Note, however, that the dynamics of a CG model are inherently only approximate. Because of the neglect of atomistic degrees of freedom, CG molecules diffuse faster compared with molecules modeled with full atomic resolution. The speedup factor sensitively depends on the details of the system. In the case of the thylakoid lipids, we previously measured a speed up factor of ∼30 based on a comparison of the mean-squared displacement curves of the CG lipids to atomistic ones.[39] Correcting for this difference, a more realistic diffusion rate for the PSII dimer is on the order of $10^{-1}\ \mu m^2\ s^{-1}$. This is definitely much higher than experimental values reported for PSII diffusion and also higher than the diffusion of other smaller proteins in the plasma membrane.[68] Measurements show that the mobility of PSII is very low, in particular, under nonstress conditions in both cyanobacteria and plants, with a diffusion constant $<2 \times 10^{-5}\ \mu m^2\ s^{-1}$ in cyanobacteria.[69,70] Monte Carlo simulations showed that PSII diffusion is severely hampered at high packing densities.[71] In our simulations only a single PSII dimer is considered; therefore, our diffusion rate represents an upper limit for the mobility of PSII at infinite dilution. Interestingly, plants can increase the protein mobility in the grana upon high light stress by changing the organization of the grana membranes.[72,73] Also, in cyanobacteria the protein mobility is increased after high light exposure. After an intense red light treatment the diffusion of all chlorophyll containing pigments is $\sim 2.3 \times 10^{-2}\ \mu m^2\ s^{-1}$.[74] Our data support that the difference in diffusivity between high and low stress conditions is likely a consequence of changes in protein packing density.

Mobility of Cofactors Is Coupled to Location Inside the Protein. The mobility of the cofactors was also assessed by means of RMSF. The cofactor RMSF was obtained after fitting the protein on the BB beads and by using the time-averaged cofactor position as the reference state. The RMSFs were calculated separately for each monomer and are shown in Figure 4 for the different types of cofactors. Average RMSF values are listed in Table S4. We recall that CHLs, PHOs, and HEMs are ligated to the protein via harmonic bonds, and thus cannot move away from their position as a whole; they are, however, to a certain extent able to tilt and rotate (cf. Table S2).

We find that the mobility of the CHLs depends on their location in the PSII complex (Figure 4). Toward the periphery of the protein the CHL molecules are more mobile; this is especially true for CHL12 that is located completely at the periphery of the complex. The centrally located CHL4 and CHL5 are very stable. The mobility of PHO is similar to the neighboring CHLs. Not surprisingly, the most mobile part within a CHL molecule is its tail, which is free to move as it is not ligated to its surroundings unlike the porphyrin ring (Table S2). The CHL tails become even more mobile when they are in contact with lipids.

It has been shown that a higher CHL mobility can broaden the absorbance spectrum for PSI and LHCII.[75−77] The higher mobility results in a larger spread of possible pigment environments, leading to more possible vibrational energy levels of the electronic ground state, which allows the CHLs to absorb photons that have a lower or higher energy than required for charge separation. It has been hypothesized that this is also the case for PSII,[78] and our data suggest that this might be particularly relevant toward the protein's periphery because there the CHL mobility is the highest; see Figure 4.

The four HEMs (two per monomer) remain tightly bound (Figure 4). The mobility of HEM41 is somewhat higher than that of HEM42. This is mainly reflecting the higher mobility of cyt b 559α and cyt b 559β, which coordinate HEM41, compared with PsbV, which coordinates HEM42.

Beta-Carotenes Are Highly Mobile and Can Exchange with Thylakoid Membrane. The BCRs have in vivo only hydrophobic interactions with the protein; therefore, we did not bind them to the complex. Consequently, they are free to move, and that is exactly what we observed. Some BCRs diffuse out of the protein complex, while others travel within the complex. In particular, the BCRs close to the PLQ exchange cavity show a high mobility (Figure 4), including the added BCRs with residue number 794 (see Supporting Information and Table S3). The high mobility could explain why these two BCRs were not properly identified in the crystal structure (with an average B factor of 60). One of the added BCRs even diffuses through the PLQ entry/exit pathway, as illustrated in Figure 5A. The lipid environment in the interfacial cleft also provides reasonable mobility to the BCRs; some of the BCRs actually change their positions in the dimer interface. They wriggle their headgroups in between the different interfacial subunits, for example, between subunits D1 and D2 or CP47 and PsbL. Furthermore, at the periphery of the complex, BCRs 649 and 650 of the right monomer and BCR 655 of the left monomer completely diffuse out of the protein into the bulk thylakoid membrane (Figure 5B). They continue diffusing around at the bilayer midplane, in agreement with the predicted location of BCR in lipid bilayers based on our previous MD simulations.[40] Eventually, two out of three BCRs reassociate with the protein. BCR649, which originates from the dimer interface, ends up in the PLQ exchange cavity of the other monomer, entering via Channel I (see Guskov et al. for the channel names[5]). BCR650 reattaches to the protein at the D2 subunit, next to PLQ channel II. In each of the five replicate simulations, we observe BCRs diffusing out of the protein complex; albeit not always the same BCRs leave the protein and not all the BCRs return back to the protein. On multiple occasions the BCRs diffuse into the PLQ exchange cavity, and

DOI: 10.1021/acs.jpcb.6b06865
J. Phys. Chem. B XXXX, XXX, XXX−XXX

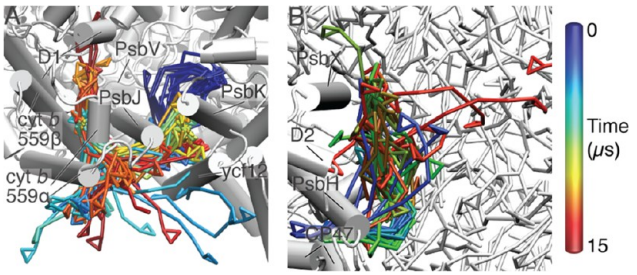

Figure 5. BCRs diffusing in and out of PSII. (A) Time series of snapshots of BCR 794 diffusing in and out of PSII. BCR 794 diffuses out of the complex between subunits PsbJ and ycf12; subsequently it reenters between cyt b 559α and PsbJ while exploring the region in between. BCR 794 is colored according to simulation time. The protein is shown from the stromal side and subunits are labeled. Note that BCR 794 was assigned as a UNL in the crystal structure; see Table S3. (B) Time series of snapshots of BCR 650 diffusing into the membrane. Stromal view on part of the PSII dimer embedded in the thylakoid membrane, both shown in white, while BCR 650 is colored according to simulation time. Subunits are labeled. The simulation times are in both panels relative to the first snapshot. The time intervals between the snapshots are not constant.

the areas around the entrances toward the PLQ channels are frequently visited by the BCRs as well.

BCRs protect PSII against photobleaching,[79] and it is therefore important that the BCRs are present in the PSII complex and stay close to the chlorophylls.[80] One would therefore not expect the BCRs to leave the protein complex. However, different from the other cofactors, BCRs are not coordinated by metal ions or charged residues to the complex; they are only stabilized by much weaker van der Waals interactions. The peripheral BCRs indeed show a higher B factor than the more shielded BCRs in the structure of Umena et al. It is therefore plausible that these BCRs are able to diffuse in and out of the PSII complex. There is experimental support for a model in which BCRs can be replaced. Isotope labeling experiments revealed that there is a continuous turnover of BCR, also under nonstressful conditions.[81] If BCRs can diffuse in and out of PSII, one would expect the presence of a pool of free BCRs in the thylakoid membrane. BCRs have been detected in the thylakoid membrane,[82] but it is not clear if these originate from PSII or are indeed free BCR molecules. To our knowledge there is no clear data on the amount of free BCR in thylakoid membranes. It has been suggested that BCR and other pigments bind at an early stage to the PSII apoprotein,[83,84] which makes the presence of a BCR pool less likely. On the contrary, Boehm et al.[84] measured a relatively high CHL/BCR ratio in isolated CP47 complexes, which is attributed to the loss or absence of BCRs, which would mean that the BCRs are not very strongly bound to the protein. Besides that, reconstitution experiments have shown that BCR does not significantly contribute to the stability of the CP43 protein,[85] suggesting that BCRs can leave the complex without any major consequences for the protein structure. More experimental and computational studies are needed to further clarify this point. It is certainly possible that the Martini force field does not capture the true dynamics of BCR in PSII. It is, however, worth considering that BCR, and possibly other cofactors, are more dynamic than conceived to us through crystal structures.

PLQ Remains Stably Bound in the Q_B Site. PSII contains two PLQs per monomer, the stationary Q_A and Q_B. Q_B becomes a PLQol after accepting two electrons and two protons. We measured the PLQs' relative mobility by measuring their RMSF.

Although Q_A remains at its binding site, as expected given its stationary role, Q_A is surprisingly mobile (see Table S5 and Figure 4). In the right monomer of the dimer simulation, the end of the Q_A tail is able to pass alongside PsbT, which has moved slightly regarding to its position in the crystal structure. The tip of the Q_A tail resides at the dimer interface for some time, but by the end of the simulation it returns back inside the monomer. Not only are the tails of the Q_A molecules mobile, but also the head groups of the molecules can change position within the binding site. The headgroup mobility seems to be unrelated to the PsbT position. The tails of the Q_B molecules are also rather mobile, but their head groups show very limited movement. In any case, the Q_B cofactors remain firmly bound, which makes sense as the cofactor is in its fully oxidized PLQ form that should stay in the binding site until it has been double-reduced toward PLQol.

In conclusion, it seems that the Q_A PLQ is able to reorient to some extent inside its binding pocket, whereas the PLQ at Q_B is rather stationary.

PSII Monomer Adopts a Tilted Orientation in the Membrane. To test if the PSII dimer and monomer behave differently, we also performed a 60 μs simulation of the monomer embedded in the thylakoid membrane. Simulation conditions were the same as for the dimer.

The PSII monomer exhibited some intriguing behavior. After ~2 μs the protein tilted in the thylakoid membrane, moving the PsbO subunit toward the membrane surface and causing substantial membrane buckling, as illustrated in Figure 6. In the

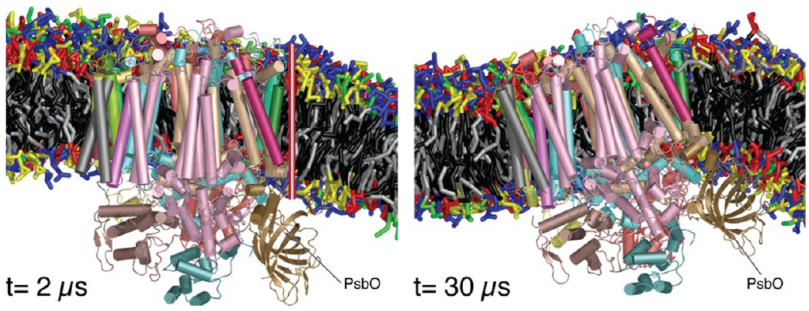

Figure 6. Tilting of PSII monomer. Snapshots of PSII-monomer in the thylakoid membrane at two different time points, the onset of tilting (t = 2 μs) and a fully tilted configuration (t = 30 μs). PsbO is marked and the dimer interface is indicated in the left panel by a gray/red line. Coloring of the protein subunits as in Figure 3.

DOI: 10.1021/acs.jpcb.6b06865
J. Phys. Chem. B XXXX, XXX, XXX−XXX

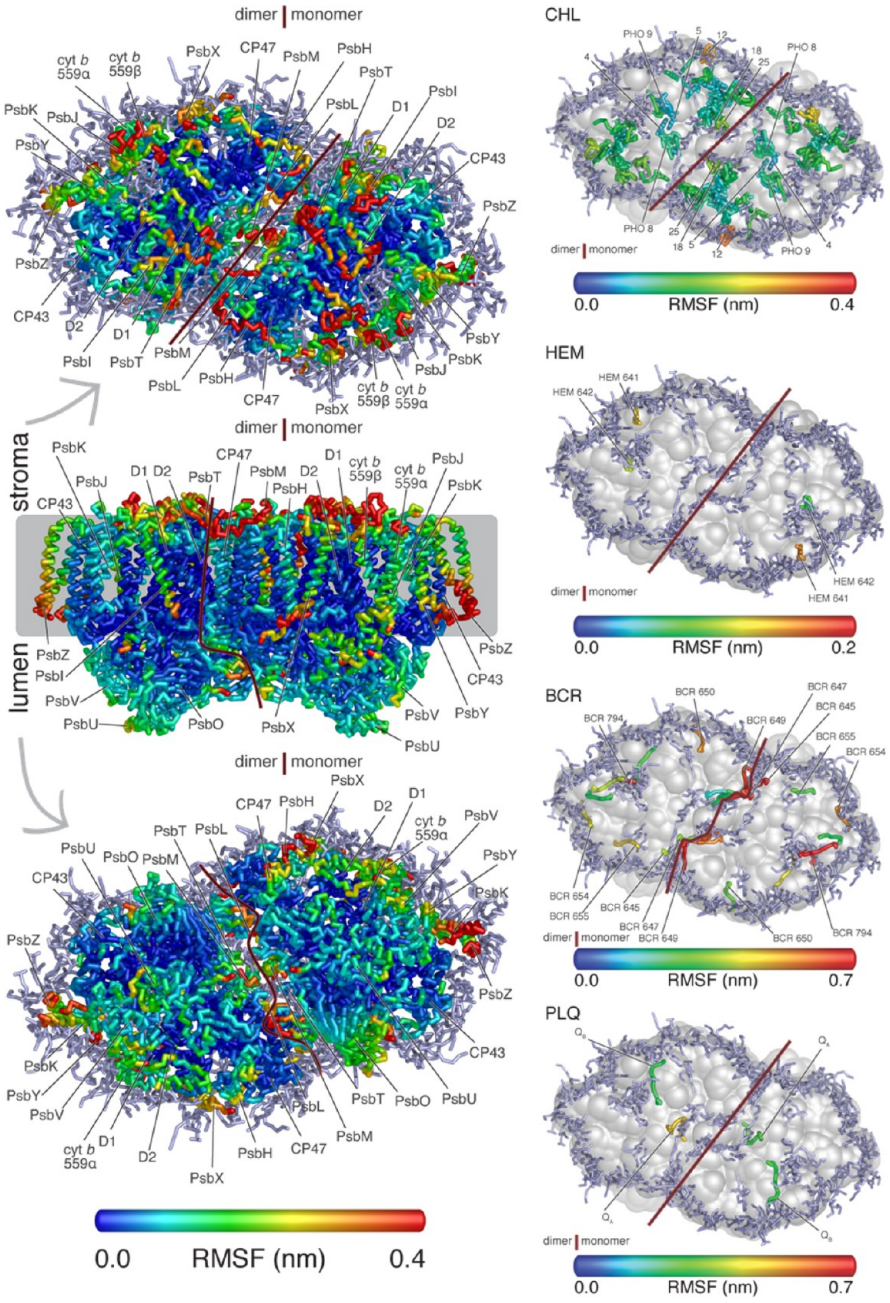

Figure 7. RMSF fluctuations of the PSII backbone (left) and the cofactors (right) of the PSII dimer and PSII monomer combined. In each panel, the left monomer is colored according to the average RMSF of the two monomers from the PSII dimer, and the right monomer is colored according to the monomer RMSF. The left side shows the fluctuations of the PSII backbone, which are capped at 0.4 nm. Lipids close to the protein are shown in light blue in the stromal and lumenal views. The various subunits are marked. The right side shows the fluctuations of the different cofactors. First panel: chlorophyll *a* (CHL) and pheophytin (PHO). Second panel: heme (HEM). Third panel: β-carotene (BCR). Fourth panel: plastoquinone (PLQ). Each cofactor is colored according to the average RMSF of the complete cofactor. All panels show a stromal view of PSII, with the protein rendered as a transparent surface and the cofactor beads colored according to their RMSF value. For clarity, the RMSF values are capped at 0.4, 0.2, and 0.7 nm for CHL/PHO, HEM, and BCR, respectively. The PLQ RMSF values are not capped. Lipids close to the protein are shown in light blue. The cofactors are labeled with their identifier; in the first panel only the CHL and PHO cofactors that are mentioned in the text are labeled.

dimer configuration the second monomer would prevent such tilting. The monomer tilting might be caused by a different shape of the monomer compared with the dimer, forcing the protein in a different orientation to release hydrophobic mismatch. Another option is that PsbO can form favorable interactions with the thylakoid lipids but only when tilting. There seem to be some interactions between the positive charged amino acids in PsbO and the negatively charged thylakoid lipids, especially SQDG.

In plants the repair cycle of PSII involves monomerization of PSII and the subsequent movement of the monomer from the grana stacks to the stroma lamellae.[86−88] We speculate that the combination of an extremely crowded membrane combined with the tendency to buckle might drive PSII monomers to diffuse toward the stromal lamellae. The monomer might not be able to tilt in the very crowded grana core,[89] but the grana margin might provide enough space for it. It would therefore be energetically favorable for the monomer to move toward the

DOI: 10.1021/acs.jpcb.6b06865
J. Phys. Chem. B XXXX, XXX, XXX−XXX

grana margin, from where it can diffuse toward the stroma lamellae. Although cyanobacteria lack grana appression and grana stacking, there is evidence that also in cyanobacteria PSII is repaired in specialized regions of the thylakoid membrane, to which PSII has to diffuse.[90]

Similar Protein and Cofactor Mobility in Monomeric and Dimeric PSII. We also compared the relative mobilities of the subunits and cofactors between the monomer and dimer configurations. The mobility of the monomer backbone is very similar to that of the dimer (Table S4, Figure 7, left panel). The average RMSF of the monomer subunits is 0.16 nm, slightly higher than the dimer, and has a maximum of 0.50 nm for the PsbH subunit. The biggest differences are found in the interfacial subunits PsbI, PsbL, PsbM, and PsbT that are significantly more mobile in the monomer. The largest part of the PsbM and PsbT helices tilts and moves a bit away from the protein; only their lumenal parts remain close to the rest of the complex.

There is no major difference between the mobility of the CHL molecules in the monomer and the dimer (Table S4, Figure 7, right panel). The mobility of the PHO porphyrin ring is also similar between monomer and dimer. In the monomer, the tail of PHO8 is able to flip into the dimer interfacial region and thereby ends up in the membrane, where it has a lot of conformational freedom, resulting in a higher RMSF (Table S4). The BCRs at the location of the dimer interface are also more mobile in the monomer. Three out of the five interfacial BCRs (BCR 645, 647, 649) diffuse out of the monomer versus one out of the dimer. Outside of the dimer interface, BCR 654 and 794 leave the complex. As with the dimer, also for the monomer a high BCR mobility is observed around the PLQ exchange cavity, and all of the BCRs that diffuse out of the complex reassociate again with the protein. The stability of the HEMs is nearly identical in the monomer and the dimer.

In the monomer, the stationary Q_A also shows a higher mobility than Q_B. This is mainly due to the movement of the interfacial helix PsbT. Although there was only a slight movement of PsbT in the dimer, in the monomer, the helix diffuses away from its initial position during the simulation. Possibly this is caused by the absence of interfacial lipids that keep the helix in place. This results in an increased conformational freedom of the Q_A tail. The fact that the mobility of Q_A is a function of the presence of PsbT is in line with experimental results that show the requirement of PsbT for stable positioning of Q_A.[91]

The overall similarity of the PSII monomer and the dimer regarding protein and cofactor mobility might be expected given that PSII monomers are capable of oxygen evolution.[87] If the intrinsic dynamics of the monomer would be very different, proper oxygen evolution would likely be hampered.

Comparison of the lateral diffusion constant between the monomer and dimer PSII shows a remarkable difference. The lateral diffusion constant for the monomer is $1 \pm 0.2\ \mu m^2\ s^{-1}$, which is significantly lower than the diffusion constant of the dimer ($2.5 \pm 0.3\ \mu m^2\ s^{-1}$) despite the smaller size of the monomer. We attribute the slow diffusional speed of the monomer to its tilted orientation in the thylakoid membrane, which increases the friction.

CONCLUSIONS

Using coarse-grained MD simulations, we characterized the behavior of PSII monomers and dimers in the thylakoid membrane on a multimicrosecond time scale. The PSII dimer appeared to be a stable complex, although one of its peripheral subunits (PsbX) detached from the complex and started to move toward PsbH. The PSII core was the most stable region of the complex, with the peripheral and interfacial residues with a higher mobility, as well as the residues lining the PLQ exchange cavity. We did not find any evidence of the involvement of PsbM in stabilizing the dimer, instead lipids squeeze into the PsbM−PsbM interface. The mobility of the cofactors depends on the type of cofactor and location in the protein. The porphyrin-based cofactors show little mobility within the complex, as they are ligated to the protein. PLQs, although free to move, remain stably bound at both the Q_A and Q_B sites. The BCRs, on the contrary, were very mobile and even diffused out of the protein complex in some cases. Our results suggest the presence of a BCR pool in the thylakoid membrane, allowing BCRs to dynamically enter and leave PSII.

Whereas the PSII dimer appears properly embedded in the thylakoid membrane, the orientation of the PSII monomer was surprising. The PSII monomer adapted a tilted conformation, with concomitant buckling of the membrane. Whether the tilting is caused by the shape of the monomer or by favorable interactions between PsbO and the membrane is not clear at this point. One may speculate the buckling behavior to be a mechanism favoring the diffusion of PSII monomers toward the grana margins as part of the PSII repair cycle. In the monomer the protein and cofactor mobility is increased around the dimer interface but is similar to the dimer in other parts of the protein. The diffusion of the monomer is, however, hampered in comparison with the dimer, probably as a result of the buckling.

Our simulations contain much more interesting information than presented here. In forthcoming work we will analyze the interactions between PSII and the thylakoid lipids and the entry and exit behavior of PLQs. Furthermore, our data could be used for an improved quantum mechanical analysis of the exciton transfer within PSII, taking into account realistic conformations of the chlorophylls. It might even be possible to calculate absorbance and fluorescence spectra. A complete all-atom model of PSII, including all cofactors and thylakoid lipids, could be constructed using efficient backmapping tools[52] and recently parametrized all-atom force fields of the cofactors and the thylakoid lipids.[39,40,92] Finally, combined with recent models of the LHCII complex[77] and PSII of higher plants,[7] detailed models of light-harvesting supercomplexes[93] could be developed following the pioneering work of the Schulten group[17] on the bacterial chromatophore.

ASSOCIATED CONTENT

Supporting Information

The Supporting Information is available free of charge on the ACS Publications website at DOI: 10.1021/acs.jpcb.6b06865.

Methodological details of the force field improvements for some of the cofactors, the approaches to stably coordinate cofactors, an overview of all the cocrystallized lipids included in our model, and analysis details as well as supporting results (RMSD and RMSF data and MSD curves). (PDF)

AUTHOR INFORMATION

Corresponding Author

*E-mail: s.j.marrink@rug.nl. Tel: +31503634457.

DOI: 10.1021/acs.jpcb.6b06865
J. Phys. Chem. B XXXX, XXX, XXX−XXX

Notes

The authors declare no competing financial interest.

■ ACKNOWLEDGMENTS

F.J.v.E. was supported by a FOM (Foundation for Fundamental Research on Matter) program. We thank Albert Guskov and Egbert Boekema for helpful discussions and Klaus Schulten for his pioneering computational work.

■ REFERENCES

(1) Blankenship, R. E. *Molecular Mechanisms of Photosynthesis*, 2nd ed.; Wiley Blackwell, 2014.
(2) Croce, R.; van Amerongen, H. Light-Harvesting and Structural Organization of Photosystem II: From Individual Complexes to Thylakoid Membrane. *J. Photochem. Photobiol., B* **2011**, *104* (1−2), 142−153.
(3) Dekker, J. P.; Boekema, E. J.; Witt, H. T.; Rögner, M. Refined Purification and Further Characterization of Oxygen-Evolving and Tris-Treated Photosystem II Particles From the Thermophilic Cyanobacterium Synechococcus Sp. *Biochim. Biophys. Acta, Bioenerg.* **1988**, *936* (3), 307−318.
(4) Pagliano, C.; Saracco, G.; Barber, J. Structural, Functional and Auxiliary Proteins of Photosystem II. *Photosynth. Res.* **2013**, *116* (2−3), 167−188.
(5) Guskov, A.; Kern, J.; Gabdulkhakov, A.; Broser, M.; Zouni, A.; Saenger, W. Cyanobacterial Photosystem II at 2.9-Å Resolution and the Role of Quinones, Lipids, Channels and Chloride. *Nat. Struct. Mol. Biol.* **2009**, *16* (3), 334−342.
(6) Umena, Y.; Kawakami, K.; Shen, J.-R.; Kamiya, N. Crystal Structure of Oxygen-Evolving Photosystem II at a Resolution of 1.9 Å. *Nature* **2011**, *473* (7345), 55−60.
(7) Wei, X.; Su, X.; Cao, P.; Liu, X.; Chang, W.; Li, M.; Zhang, X.; Liu, Z. Structure of Spinach Photosystem II−LHCII Supercomplex at 3.2 Å Resolution. *Nature* **2016**, *534* (7605), 69−74.
(8) Fromme, P.; Grotjohann, I. Structure of Photosystems I and II. *Results Probl. Cell Differ.* **2008**, *45*, 33−72.
(9) Lea-Smith, D. J.; Bombelli, P.; Vasudevan, R.; Howe, C. J. Photosynthetic, Respiratory and Extracellular Electron Transport Pathways in Cyanobacteria. *Biochim. Biophys. Acta, Bioenerg.* **2016**, *1857* (3), 247−255.
(10) Garab, G. Self-Assembly and Structural-Functional Flexibility of Oxygenic Photosynthetic Machineries: Personal Perspectives. *Photosynth. Res.* **2016**, *127* (1), 131−150.
(11) Kouřil, R.; Dekker, J. P.; Boekema, E. J. Supramolecular Organization of Photosystem II in Green Plants. *Biochim. Biophys. Acta, Bioenerg.* **2012**, *1817* (1), 2−12.
(12) Guskov, A.; Gabdulkhakov, A.; Broser, M.; Glöckner, C.; Hellmich, J.; Kern, J.; Frank, J.; Müh, F.; Saenger, W.; Zouni, A. Recent Progress in the Crystallographic Studies of Photosystem II. *ChemPhysChem* **2010**, *11* (6), 1160−1171.
(13) Romero, E.; Augulis, R.; Novoderezhkin, V. I.; Ferretti, M.; Thieme, J.; Zigmantas, D.; van Grondelle, R. Quantum Coherence in Photosynthesis for Efficient Solar Energy Conversion. *Nat. Phys.* **2014**, *10* (9), 676−682.
(14) Ingólfsson, H. I.; Arnarez, C.; Periole, X.; Marrink, S. J. Computational "Microscopy" of Cellular Membranes. *J. Cell Sci.* **2016**, *129* (2), 257−268.
(15) Stansfeld, P. J.; Sansom, M. S. P. Molecular Simulation Approaches to Membrane Proteins. *Structure* **2011**, *19* (11), 1562−1572.
(16) Mayne, C. G.; Arcario, M. J.; Mahinthichaichan, P.; Baylon, J. L.; Vermaas, J. V.; Navidpour, L.; Wen, P.-C.; Thangapandian, S.; Tajkhorshid, E. The Cellular Membrane as a Mediator for Small Molecule Interaction with Membrane Proteins. *Biochim. Biophys. Acta, Biomembr.* **2016**, *1858*, 2290.
(17) Sener, M. K.; Olsen, J. D.; Hunter, C. N.; Schulten, K. Atomic-Level Structural and Functional Model of a Bacterial Photosynthetic Membrane Vesicle. *Proc. Natl. Acad. Sci. U. S. A.* **2007**, *104* (40), 15723−15728.
(18) Chandler, D. E.; Strümpfer, J.; Sener, M.; Scheuring, S.; Schulten, K. Light Harvesting by Lamellar Chromatophores in Rhodospirillum Photometricum. *Biophys. J.* **2014**, *106* (11), 2503−2510.
(19) Vassiliev, S.; Comte, P.; Mahboob, A.; Bruce, D. Tracking the Flow of Water Through Photosystem II Using Molecular Dynamics and Streamline Tracing. *Biochemistry* **2010**, *49* (9), 1873−1881.
(20) Vassiliev, S.; Zaraiskaya, T.; Bruce, D. Exploring the Energetics of Water Permeation in Photosystem II by Multiple Steered Molecular Dynamics Simulations. *Biochim. Biophys. Acta, Bioenerg.* **2012**, *1817* (9), 1671−1678.
(21) Gabdulkhakov, A. G.; Kljashtorny, V. G.; Dontsova, M. V. Molecular Dynamics Studies of Pathways of Water Movement in Cyanobacterial Photosystem II. *Crystallogr. Rep.* **2015**, *60* (1), 83−89.
(22) Ogata, K.; Yuki, T.; Hatakeyama, M.; Uchida, W.; Nakamura, S. All-Atom Molecular Dynamics Simulation of Photosystem II Embedded in Thylakoid Membrane. *J. Am. Chem. Soc.* **2013**, *135* (42), 15670−15673.
(23) Zhang, L.; Silva, D.-A.; Zhang, H.; Yue, A.; Yan, Y.; Huang, X. Dynamic Protein Conformations Preferentially Drive Energy Transfer Along the Active Chain of the Photosystem II Reaction Centre. *Nat. Commun.* **2014**, *5*, 4170.
(24) Ingólfsson, H. I.; López, C. A.; Uusitalo, J. J.; de Jong, D. H.; Gopal, S. M.; Periole, X.; Marrink, S. J. The Power of Coarse Graining in Biomolecular Simulations. *WIRES Comput. Mol. Science* **2014**, *4* (3), 225−248.
(25) Cascella, M.; Vanni, S. Toward Accurate Coarse-Graining Approaches for Protein and Membrane Simulations. *Chem. Mod.* **2015**, *12*, 1−52.
(26) Marrink, S. J.; Tieleman, D. P. Perspective on the Martini Model. *Chem. Soc. Rev.* **2013**, *42* (16), 6801−6822.
(27) Arnarez, C.; Mazat, J.-P.; Elezgaray, J.; Marrink, S. J.; Periole, X. Evidence for Cardiolipin Binding Sites on the Membrane-Exposed Surface of the Cytochrome bc_1. *J. Am. Chem. Soc.* **2013**, *135* (8), 3112−3120.
(28) Hedger, G.; Shorthouse, D.; Koldsø, H.; Sansom, M. S. P. Free Energy Landscape of Lipid Interactions with Regulatory Binding Sites on the Transmembrane Domain of the EGF Receptor. *J. Phys. Chem. B* **2016**, *120*, 8154.
(29) Arnarez, C.; Marrink, S. J.; Periole, X. Molecular Mechanism of Cardiolipin-Mediated Assembly of Respiratory Chain Supercomplexes. *Chem. Sci.* **2016**, *7*, 4435−4443.
(30) Periole, X.; Knepp, A. M.; Sakmar, T. P.; Marrink, S. J.; Huber, T. Structural Determinants of the Supramolecular Organization of G Protein-Coupled Receptors in Bilayers. *J. Am. Chem. Soc.* **2012**, *134* (26), 10959−10965.
(31) Prasanna, X.; Chattopadhyay, A.; Sengupta, D. Cholesterol Modulates the Dimer Interface of the B2-Adrenergic Receptor via Cholesterol Occupancy Sites. *Biophys. J.* **2014**, *106* (6), 1290−1300.
(32) Jeon, J.-H.; Javanainen, M.; Martinez-Seara, H.; Metzler, R.; Vattulainen, I. Protein Crowding in Lipid Bilayers Gives Rise to Non-Gaussian Anomalous Lateral Diffusion of Phospholipids and Proteins. *Phys. Rev. X* **2016**, *6* (2), 021006.
(33) Ingólfsson, H. I.; Melo, M. N.; van Eerden, F. J.; Arnarez, C.; López, C. A.; Wassenaar, T. A.; Periole, X.; de Vries, A. H.; Tieleman, D. P.; Marrink, S. J. Lipid Organization of the Plasma Membrane. *J. Am. Chem. Soc.* **2014**, *136* (41), 14554−14559.
(34) Koldsø, H.; Sansom, M. S. P. Organization and Dynamics of Receptor Proteins in a Plasma Membrane. *J. Am. Chem. Soc.* **2015**, *137* (46), 14694−14704.
(35) Sakurai, I.; Shen, J.-R.; Leng, J.; Ohashi, S.; Kobayashi, M.; Wada, H. Lipids in Oxygen-Evolving Photosystem II Complexes of Cyanobacteria and Higher Plants. *J. Biochem.* **2006**, *140* (2), 201−209.
(36) de Jong, D. H.; Singh, G.; Bennett, W. F. D.; Arnarez, C.; Wassenaar, T. A.; Schäfer, L. V.; Periole, X.; Tieleman, D. P.; Marrink, S. J. Improved Parameters for the Martini Coarse-Grained Protein Force Field. *J. Chem. Theory Comput.* **2013**, *9* (1), 687−697.

DOI: 10.1021/acs.jpcb.6b06865
J. Phys. Chem. B XXXX, XXX, XXX−XXX

(37) Periole, X.; Cavalli, M.; Marrink, S.-J.; Ceruso, M. A. Combining an Elastic Network with a Coarse-Grained Molecular Force Field: Structure, Dynamics, and Intermolecular Recognition. *J. Chem. Theory Comput.* **2009**, *5* (9), 2531−2543.
(38) López, C. A.; Sovova, Z.; van Eerden, F. J.; de Vries, A. H.; Marrink, S. J. Martini Force Field Parameters for Glycolipids. *J. Chem. Theory Comput.* **2013**, *9* (3), 1694−1708.
(39) van Eerden, F. J.; de Jong, D. H.; de Vries, A. H.; Wassenaar, T. A.; Marrink, S. J. Characterization of Thylakoid Lipid Membranes From Cyanobacteria and Higher Plants by Molecular Dynamics Simulations. *Biochim. Biophys. Acta, Biomembr.* **2015**, *1848* (6), 1319−1330.
(40) de Jong, D. H.; Liguori, N.; van den Berg, T.; Arnarez, C.; Periole, X.; Marrink, S. J. Atomistic and Coarse Grain Topologies for the Cofactors Associated with the Photosystem II Core Complex. *J. Phys. Chem. B* **2015**, *119* (25), 7791−7803.
(41) Marrink, S. J.; Risselada, H. J.; Yefimov, S.; Tieleman, D. P.; de Vries, A. H. The MARTINI Force Field: Coarse Grained Model for Biomolecular Simulations. *J. Phys. Chem. B* **2007**, *111* (27), 7812−7824.
(42) Hess, B.; Kutzner, C.; van der Spoel, D.; Lindahl, E. GROMACS 4: Algorithms for Highly Efficient, Load-Balanced, and Scalable Molecular Simulation. *J. Chem. Theory Comput.* **2008**, *4* (3), 435−447.
(43) Bussi, G.; Donadio, D.; Parrinello, M. Canonical Sampling Through Velocity Rescaling. *J. Chem. Phys.* **2007**, *126* (1), 014101.
(44) Berendsen, H.; Postma, J.; van Gunsteren, W. F.; DiNola, A.; Haak, J. R. Molecular Dynamics with Coupling to an External Bath. *J. Chem. Phys.* **1984**, *81* (8), 3684−3690.
(45) Guex, N.; Peitsch, M. C. SWISS-MODEL and the Swiss-Pdb Viewer: an Environment for Comparative Protein Modeling. *Electrophoresis* **1997**, *18* (15), 2714−2723.
(46) Fiser, A.; Sali, A. ModLoop: Automated Modeling of Loops in Protein Structures. *Bioinformatics* **2003**, *19* (18), 2500−2501.
(47) Humphrey, W.; Dalke, A.; Schulten, K. VMD: Visual Molecular Dynamics. *J. Mol. Graphics* **1996**, *14* (1), 33−38.
(48) Lomize, M. A.; Lomize, A. L.; Pogozheva, I. D.; Mosberg, H. I. OPM: Orientations of Proteins in Membranes Database. *Bioinformatics* **2006**, *22* (5), 623−625.
(49) Schrödinger, LLC. *The PyMOL Molecular Graphics System*, Version 1.7.0.0, 2010.
(50) Kabsch, W.; Sander, C. Dictionary of Protein Secondary Structure: Pattern Recognition of Hydrogen-Bonded and Geometrical Features. *Biopolymers* **1983**, *22* (12), 2577−2637.
(51) Monticelli, L.; Kandasamy, S. K.; Periole, X.; Larson, R. G.; Tieleman, D. P.; Marrink, S.-J. The MARTINI Coarse-Grained Force Field: Extension to Proteins. *J. Chem. Theory Comput.* **2008**, *4* (5), 819−834.
(52) Saito, K.; Rutherford, A. W.; Ishikita, H. Mechanism of Proton-Coupled Quinone Reduction in Photosystem II. *Proc. Natl. Acad. Sci. U. S. A.* **2013**, *110* (3), 954−959.
(53) Wassenaar, T. A.; Pluhackova, K.; Böckmann, R. A.; Marrink, S. J.; Tieleman, D. P. Going Backward: a Flexible Geometric Approach to Reverse Transformation From Coarse Grained to Atomistic Models. *J. Chem. Theory Comput.* **2014**, *10* (2), 676−690.
(54) Wassenaar, T. A.; Ingólfsson, H. I.; Böckmann, R. A.; Tieleman, D. P.; Marrink, S. J. Computational Lipidomics with Insane: a Versatile Tool for Generating Custom Membranes for Molecular Simulations. *J. Chem. Theory Comput.* **2015**, *11*, 2144−2155.
(55) Koike, H.; Hanssum, B.; Inoue, Y.; Renger, G. Temperature Dependence of S-State Transition in a Thermophilic Cyanobacterium, Synechococcus Vulcanus Copeland Measured by Absorption Changes in the Ultraviolet Region. *Biochim. Biophys. Acta, Bioenerg.* **1987**, *893*, 524.
(56) Schneider, B.; Gelly, J. C.; de Brevern, A. G.; Černý, J. Local Dynamics of Proteins and DNA Evaluated From Crystallographic B Factors. *Acta Crystallogr., Sect. D: Biol. Crystallogr.* **2014**, *70*, 2413−2419.
(57) Loll, B.; Kern, J.; Saenger, W.; Zouni, A.; Biesiadka, J. Towards Complete Cofactor Arrangement in the 3.0 a Resolution Structure of Photosystem II. *Nature* **2005**, *438* (7070), 1040−1044.
(58) Shi, L.-X.; Hall, M.; Funk, C.; Schröder, W. P. Photosystem II, a Growing Complex: Updates on Newly Discovered Components and Low Molecular Mass Proteins. *Biochim. Biophys. Acta, Bioenerg.* **2012**, *1817* (1), 13−25.
(59) Ohad, I.; Dal Bosco, C.; Herrmann, R. G.; Meurer, J. Photosystem II Proteins PsbL and PsbJ Regulate Electron Flow to the Plastoquinone Pool. *Biochemistry* **2004**, *43* (8), 2297−2308.
(60) Katoh, H.; Ikeuchi, M. Targeted Disruption of psbX and Biochemical Characterization of Photosystem II Complex in the Thermophilic Cyanobacterium Synechococcus Elongatus. *Plant Cell Physiol.* **2001**, *42* (2), 179−188.
(61) Kern, J.; Guskov, A. Lipids in Photosystem II: Multifunctional Cofactors. *J. Photochem. Photobiol., B* **2011**, *104* (1−2), 19−34.
(62) Iwai, M.; Katoh, H.; Katayama, M.; Ikeuchi, M. PSII-Tc Protein Plays an Important Role in Dimerization of Photosystem II. *Plant Cell Physiol.* **2004**, *45* (12), 1809−1816.
(63) Kawakami, K.; Umena, Y.; Iwai, M.; Kawabata, Y.; Ikeuchi, M.; Kamiya, N.; Shen, J.-R. Roles of PsbI and PsbM in Photosystem II Dimer Formation and Stability Studied by Deletion Mutagenesis and X-Ray Crystallography. *Biochim. Biophys. Acta, Bioenerg.* **2011**, *1807* (3), 319−325.
(64) Bentley, F. K.; Luo, H.; Dilbeck, P.; Burnap, R. L.; Eaton-Rye, J. J. Effects of Inactivating psbM and psbT on Photodamage and Assembly of Photosystem II in Synechocystis Sp. PCC 6803†. *Biochemistry* **2008**, *47* (44), 11637−11646.
(65) Umate, P.; Schwenkert, S.; Karbat, I.; Dal Bosco, C.; Mlcòchová, L.; Volz, S.; Zer, H.; Herrmann, R. G.; Ohad, I.; Meurer, J. Deletion of PsbM in Tobacco Alters the QB Site Properties and the Electron Flow Within Photosystem II. *J. Biol. Chem.* **2007**, *282* (13), 9758−9767.
(66) Watanabe, M.; Iwai, M.; Narikawa, R.; Ikeuchi, M. Is the Photosystem II Complex a Monomer or a Dimer? *Plant Cell Physiol.* **2009**, *50* (9), 1674−1680.
(67) Nath, K.; Jajoo, A.; Poudyal, R. S.; Timilsina, R.; Park, Y. S.; Aro, E.-M.; Nam, H. G.; Lee, C.-H. Towards a Critical Understanding of the Photosystem II Repair Mechanism and Its Regulation During Stress Conditions. *FEBS Lett.* **2013**, *587* (21), 3372−3381.
(68) Lippincott-Schwartz, J.; Snapp, E.; Kenworthy, A. Studying Protein Dynamics in Living Cells. *Nat. Rev. Mol. Cell Biol.* **2001**, *2* (6), 444−456.
(69) Sarcina, M.; Mullineaux, C. W. Mobility of the IsiA Chlorophyll-Binding Protein in Cyanobacterial Thylakoid Membranes. *J. Biol. Chem.* **2004**, *279* (35), 36514−36518.
(70) Kirchhoff, H.; Haferkamp, S.; Allen, J. F.; Epstein, D. B. A.; Mullineaux, C. W. Protein Diffusion and Macromolecular Crowding in Thylakoid Membranes. *Plant Physiol.* **2008**, *146* (4), 1571−1578.
(71) Kirchhoff, H.; Tremmel, I. G.; Haase, W.; Kubitscheck, U. Supramolecular Photosystem II Organization in Grana Thylakoid Membranes: Evidence for a Structured Arrangement†. *Biochemistry* **2004**, *43* (28), 9204−9213.
(72) Herbstová, M.; Tietz, S.; Kinzel, C.; Turkina, M. V.; Kirchhoff, H. Architectural Switch in Plant Photosynthetic Membranes Induced by Light Stress. *Proc. Natl. Acad. Sci. U. S. A.* **2012**, *109* (49), 20130−20135.
(73) Goral, T. K.; Johnson, M. P.; Brain, A. P. R.; Kirchhoff, H.; Ruban, A. V.; Mullineaux, C. W. Visualizing the Mobility and Distribution of Chlorophyll Proteins in Higher Plant Thylakoid Membranes: Effects of Photoinhibition and Protein Phosphorylation. *Plant J.* **2010**, *62* (6), 948−959.
(74) Sarcina, M.; Bouzovitis, N.; Mullineaux, C. W. Mobilization of Photosystem II Induced by Intense Red Light in the Cyanobacterium Synechococcus Sp PCC7942. *Plant Cell* **2006**, *18* (2), 457−464.
(75) Pålsson, L.-O.; Flemming, C.; Gobets, B.; van Grondelle, R.; Dekker, J. P.; Schlodder, E. Energy Transfer and Charge Separation in Photosystem I: P700 Oxidation Upon Selective Excitation of the Long-Wavelength Antenna Chlorophylls of Synechococcus Elongatus. *Biophys. J.* **1998**, *74* (5), 2611−2622.

DOI: 10.1021/acs.jpcb.6b06865
J. Phys. Chem. B XXXX, XXX, XXX−XXX

(76) Schlodder, E.; Lendzian, F.; Meyer, J.; Çetin, M.; Brecht, M.; Renger, T.; Karapetyan, N. V. Long-Wavelength Limit of Photochemical Energy Conversion in Photosystem I. *J. Am. Chem. Soc.* **2014**, *136* (10), 3904−3918.
(77) Liguori, N.; Periole, X.; Marrink, S. J.; Croce, R. From Light-Harvesting to Photoprotection: Structural Basis of the Dynamic Switch of the Major Antenna Complex of Plants (LHCII). *Sci. Rep.* **2015**, *5*, 15661.
(78) Stones, R.; Hossein-Nejad, H.; van Grondelle, R. How a Structured Vibrational Environment Controls the Performance of a Photosystem II Reaction Centre-Based Photocell. *arXiv:1601.05260*. 2016.
(79) Telfer, A. Singlet Oxygen Production by PSII Under Light Stress: Mechanism, Detection and the Protective Role of B-Carotene. *Plant Cell Physiol.* **2014**, *55* (7), 1216−1223.
(80) Pospíšil, P.; Prasad, A. Formation of Singlet Oxygen and Protection Against Its Oxidative Damage in Photosystem II Under Abiotic Stress. *J. Photochem. Photobiol., B* **2014**, *137*, 39−48.
(81) Beisel, K. G.; Jahnke, S.; Hofmann, D.; Köppchen, S.; Schurr, U.; Matsubara, S. Continuous Turnover of Carotenes and Chlorophyll a in Mature Leaves of Arabidopsis Revealed by 14CO2 Pulse-Chase Labeling. *Plant Physiol.* **2010**, *152* (4), 2188−2199.
(82) Juhler, R. K.; Andreasson, E.; Yu, S.-G.; Albertsson, P.-Å. Composition of Photosynthetic Pigments in Thylakoid Membrane Vesicles From Spinach. *Photosynth. Res.* **1993**, *35* (2), 171−178.
(83) Nickelsen, J.; Rengstl, B. Photosystem II Assembly: From Cyanobacteria to Plants. *Annu. Rev. Plant Biol.* **2013**, *64* (1), 609−635.
(84) Boehm, M.; Romero, E.; Reisinger, V.; Yu, J.; Komenda, J.; Eichacker, L. A.; Dekker, J. P.; Nixon, P. J. Investigating the Early Stages of Photosystem II Assembly in Synechocystis Sp. PCC 6803: Isolation of CP47 and CP43 Complexes. *J. Biol. Chem.* **2011**, *286* (17), 14812−14819.
(85) Liu, J.; Xie, S.-S.; Luo, Y.; Zhu, G.-F.; Du, L.-F. Soluble Expression of Spinach psbC Gene in Escherichia Coli and in Vitro Reconstitution of CP43 Coupled with Chlorophyll a Only. *Plant Physiol. Biochem.* **2014**, *79*, 19−24.
(86) Aro, E. M.; Suorsa, M.; Rokka, A.; Allahverdiyeva, Y.; Paakkarinen, V.; Saleem, A.; Battchikova, N.; Rintamäki, E. Dynamics of Photosystem II: a Proteomic Approach to Thylakoid Protein Complexes. *J. Exp. Botany* **2005**, *56* (411), 347−356.
(87) Danielsson, R.; Suorsa, M.; Paakkarinen, V.; Albertsson, P.-Å.; Styring, S.; Aro, E.-M.; Mamedov, F. Dimeric and Monomeric Organization of Photosystem II. Distribution of Five Distinct Complexes in the Different Domains of the Thylakoid Membrane. *J. Biol. Chem.* **2006**, *281* (20), 14241−14249.
(88) Yoshioka, M.; Nakayama, Y.; Yoshida, M.; Ohashi, K.; Morita, N.; Kobayashi, H.; Yamamoto, Y. Quality Control of Photosystem II: FtsH Hexamers Are Localized Near Photosystem II at Grana for the Swift Repair of Damage. *J. Biol. Chem.* **2010**, *285* (53), 41972−41981.
(89) Kirchhoff, H.; Mukherjee, U.; Galla, H. J. Molecular Architecture of the Thylakoid Membrane: Lipid Diffusion Space for Plastoquinone. *Biochemistry* **2002**, *41* (15), 4872−4882.
(90) Sacharz, J.; Bryan, S. J.; Yu, J.; Burroughs, N. J.; Spence, E. M.; Nixon, P. J.; Mullineaux, C. W. Sub-Cellular Location of FtsH Proteases in the Cyanobacterium Synechocystis Sp. PCC 6803 Suggests Localised PSII Repair Zones in the Thylakoid Membranes. *Mol. Microbiol.* **2015**, *96* (3), 448−462.
(91) Ohnishi, N.; Kashino, Y.; Satoh, K.; Ozawa, S.-I.; Takahashi, Y. Chloroplast-Encoded Polypeptide PsbT Is Involved in the Repair of Primary Electron Acceptor QA of Photosystem II During Photoinhibition in Chlamydomonas Reinhardtii. *J. Biol. Chem.* **2006**, *282* (10), 7107−7115.
(92) Debnath, A.; Wiegand, S.; Paulsen, H.; Kremer, K.; Peter, C. Derivation of Coarse-Grained Simulation Models of Chlorophyll Molecules in Lipid Bilayers for Applications in Light Harvesting Systems. *Phys. Chem. Chem. Phys.* **2015**, *17* (34), 22054−22063.
(93) Lee, C.-K.; Pao, C.-W.; Smit, B. PSII−LHCII Supercomplex Organizations in Photosynthetic Membrane by Coarse-Grained Simulation. *J. Phys. Chem. B* **2015**, *119* (10), 3999−4008.

DOI: 10.1021/acs.jpcb.6b06865
J. Phys. Chem. B XXXX, XXX, XXX−XXX